Improving tribocorrosion resistance of a medical grade CoCrMo alloy by the novel HIPIMS nitriding technique

PURANDARE, Y., SHUKLA, K., SUGUMARAN, A., EHIASARIAN, A., KHAN, I. and HOVSEPIAN, Papken <http://orcid.org/0000-0002-1047-0407>

Journal of Science: Advanced Materials and Devices 8 (2023) 100570

Contents lists available at ScienceDirect

Journal of Science: Advanced Materials and Devices

journal homepage: www.elsevier.com/locate/jsamd

Original Article

Improving tribocorrosion resistance of a medical grade CoCrMo alloy by the novel HIPIMS nitriding technique

Y. Purandare [a, *], K. Shukla [a], A. Sugumaran [a], A. Ehiasarian [a], I. Khan [b], P. Hovsepian [a]

[a] National HIPIMS Technology Centre, MERI, Sheffield Hallam University, UK
[b] Zimmer-Biomet UK Limited, UK

ARTICLE INFO

Article history:
Received 23 January 2023
Received in revised form
6 April 2023
Accepted 2 May 2023
Available online 3 May 2023

Keywords:
CoCrMo
HIPIMS
Nitriding
Sliding-wear-corrosion
Tribocorrosion
Friction

ABSTRACT

In this work, tribocorrosion performance of the High Power Impulse Magnetron Sputtering (HIPIMS) nitrided (F75) CoCrMo alloys was examined with the help of sliding wear corrosion experiments carried out in Hank's solution. Results indicate that under Open Circuit Potentials (OCP), both nitrided and the untreated specimens exhibited near similar Sliding-Wear-Corrosion coefficient (K_{SWC}) values (6.52×10^{-15} and 3.95×10^{-15} $m^3N^{-1}m^{-1}$ respectively). However, the benefits of HIPIMS nitriding were evident under accelerated corrosion (anodic potentials) and passivating conditions. K_{SWC} values of the nitrided specimens were an order of magnitude lower (6.41×10^{-15} $m^3N^{-1}m^{-1}$) than the untreated specimens (3.4×10^{-14} $m^3N^{-1}m^{-1}$), indicating that nitrided surfaces had higher resistance against tribocorrosive mechanisms. This superior performance was attributed to the formation of a nitrided microstructure consisting mainly of expanded austenite (γ_N) without the formation of the detrimental CrN phase, which resulted in high hardness and sustained resistance to corrosion. A rationale for lower synergy between wear and corrosion and its relation to the nitride microstructure has been presented.

1. Introduction

CoCrMo alloys have been a popular choice as a biomaterial for manufacturing artificial joints, dental implants and associated accessories such as spinal segments, bone plates and screws [1–3]. However, these implants, especially metal-on-metal (MoM) versions, have shown a considerable rejection rate, with most of the failures associated with high wear and corrosion of the bearing surfaces in contact [3,4]. Corrosion of the surfaces can lead to higher roughness, eventually leading to a vicious cycle of higher friction coefficients followed by wear and that presence of proteins and absorbed protein layers can lead to higher corrosion of CoCrMo alloys [5]. There have been several reports that CoCrMo is susceptible to microstructural changes in the contact zones when it is under dynamic loading conditions similar to those experienced when undergoing wear [6,7]. However, the effect of these microstructural changes on the wear resistance is still unclear. As a result, these alloys have been a subject of intense research, wherein various surface treatments such as plasma nitriding [8–11] or deposition of hard coatings [12–15] have been explored with the main aim of enhancing wear and corrosion resistance of these alloys.

The novel High Power Impulse Magnetron Sputtering (HIPIMS) technique produces highly ionized plasma and is recognized as an advantageous technique for coating deposition [16]. In 2005 however, Prof. A.P. Ehiasarian and Prof. P. Eh. Hovsepian developed first time a plasma nitriding technology which utilizes HIPIMS discharge [17]. Recently the technology was successfully used to nitride a medical grade low carbon CoCrMo alloy (F75) [18–22]. Using this HIPIMS Low Pressure Nitriding technique (henceforth denoted as HLPN) brings valuable advantages. HLPN can be carried out in the same hardware setup as that for coating deposition, however, at lower working pressures (typically in the range of 10^{-3} mbar) as compared to state-of-the-art plasma nitriding. This facilitates hardware simplicity as both the nitriding and coating process approach, known as the duplex process, can be carried out without interruption in one machine. In HIPIMS, due to the application of high powers in small pulses (typically ranging around 20–200 μs), a dense plasma is generated, which is highly ionized resulting in a higher proportion of molecular (N^{2+}) and atomic

* Corresponding author. National HIPIMS Technology Centre, Materials and Engineering Research Institute, City Campus, Sheffield Hallam University, Howard street, Sheffield, S1 1WB, UK.
E-mail address: y.purandare@shu.ac.uk (Y. Purandare).
Peer review under responsibility of Vietnam National University, Hanoi.

https://doi.org/10.1016/j.jsamd.2023.100570

nitrogen (N^+) in the plasma [16]. This leads to a greater amount of nitrogen species diffusing into the substrate when a suitable bias voltage is applied.

Thus, the process becomes more efficient and a thicker nitriding layer can be achieved in significantly less time (about 4 times faster) and at lower temperatures (in the range of 450 °C) as compared to conventional gas plasma nitriding plasma process [22].

The previous works have demonstrated that HLPN of F75 alloys carried out at a nitriding voltage of −900 V resulted in the best combination of hardness, toughness, wear and corrosion resistance (analysed independently) offered by the nitrided layer [19,20]. The enhancement in these properties were attributed to its superior microstructure which consisted of a thicker S phase diffusion based Co_4N near the substrate interface followed by a thick and uniform $Co_{2\text{-}3}N$ compound layer on the top.

Even if a material possess high wear resistance or corrosion resistance or a combination of both of these, it will not necessarily bestow high tribocorrosion resistance in it. Hence, tribocorrosion (combined wear and corrosion) studies has received a lot of attention in the recent years as it is very system dependent. There is a general consensus that nitriding improves wear resistance of CoCrMo alloys, however there is a considerable ambiguity on the corrosion protection offered by nitrided CoCrMo surfaces with no clear consensus on its benefits [23–26]. In practical applications, such as prosthetic joints or dental implants, wear and corrosion are intertwined and as a result the surface undergoes through complex tribocorrosive material removal mechanisms. Both, wear and corrosion can have significant influence on each other as well as on other properties such as friction, wear mechanisms, microstructure, pH and electrochemical potentials and many more [27–29]. As a result, in most cases, the resultant material degradation is more than the mathematical sum of the individual phenomenon.

For instance, a high synergy between wear and corrosion leading to higher wastage rates was reported by Lutz and Mandl [30] when CoCrMo alloys were nitrided using the Plasma Immersion Ion Implantation (PIII) technique at elevated temperatures (530 °C and 570 °C) as compared to process temperatures of 390 °C, and 405 °C. The authors suggested that the loss of corrosion was due to the depletion of Cr from the matrix leading to the formation of CrN at elevated temperatures and that led to a higher synergy between wear and corrosion. Depletion of corrosion resistance due to formation of CrN at higher nitrogen doses was also reported by Guo et al. [31]. However, the same study (tribocorrosion studies in new born bovine serum) also revealed higher E_{Corr} potentials and reduced wear track volumes with higher nitrogen ion dosages suggesting that the overall higher tribocorrosion resistance obtained was due to higher hardness rather than higher corrosion resistance. A similar improvement in tribocorrosion resistance due to improved hardness was reported by Wang et al. [32]. and Zhao et al. [33] even though their nitrided samples exhibited higher corrosion currents and friction coefficients as compared to untreated CoCrMo alloys. Even though there is a lot of literature which reports improvements in individual wear and corrosion resistance of CoCr(Mo) alloys due to nitriding, in all instances, they have been characterized separately. Through the very limited literature available on combined studies, it is evident that tribocorrosion resistance achieved by nitriding of CoCr(Mo) alloys is very subjective and there is a clear need to scrutinize the tribocorrosive response of these engineered surfaces.

HLPN technique looks very promising in improving the wear and corrosion resistance of CoCr(Mo) alloys. However this novel technique needs further investigation on its offering from a tribocorrosive perspective. Hence, in this work, HLPN treated medical grade low carbon CoCrMo (F75) alloy specimens (henceforth referred to as nitrided) and untreated condition, were subjected to combined sliding wear and corrosion experiments. Experiments were performed at different electrochemical potentials in a simulated bio fluid environment (Hank's solution) with an emphasis to find the response and wear mechanisms of these materials.

2. Experimental

2.1. HLPN process

F75 CoCrMo alloy discs (25 mm diameter and 6 mm thickness) were nitrided using an industrial scale PVD machine (Hauzer techno Coating 100–4, the Netherlands) enabled with HIPIMS technology at the National HIPIMS Technology Centre at Sheffield Hallam University, UK. The system is equipped with two HIPIMS power supplies energising the sputtering sources and a dedicated bias power supply [34] (Hüttinger Elektronik Sp. z o.o., Warsaw, Poland) connected to the substrate turntable which held the test specimens. After preparation (metallurgically polished to a mirror like surface finish followed by industrial cleaning using alkali solutions) the coupons were loaded on a centrally placed rotating table capable of undergoing 3-fold planetary rotation. Prior to the nitriding process, the sample surfaces were etched (cleaned of hydroxides) with the help of an intense bombardment from highly energetic and ionised HIPIMS plasma sustained on a chromium (Cr) target. Plasma nitriding was carried out in mixed nitrogen and hydrogen, N_2/H_2 (85:15), gas atmosphere using HIPIMS discharge sustained on two (one Cr and one Nb) targets and two UBM (one Cr and one Nb) targets for 4 h at a process temperature of 400 °C. The detailed description of the HLPN process at different nitriding voltages (−500 to −1100 V representing increasing bombarding energies of the ionised flux) has been described in detail in a previous publication [18]. It was found out that, employing a nitriding voltage of −900 V promotes the growth of a desirable layer microstructure possessing a right combination of high hardness, improved toughness, higher impact fatigue and fracture toughness along with improved corrosion resistance [19,20]. Thus, in continuation with the studies, for the current work specimen nitrided at −900 V coupons were chosen for analysing their tribocorrosion performance.

2.2. Sliding wear-corrosion experiments (SWC)

Sliding wear-corrosion experiments were conducted on a modified pin on disk tribometer (tribometer, Anton Paar- CSEM Instruments, Switzerland). The apparatus consists of a static counterpart (6 mm Al_2O_3 ball-hardness 1800 HV held in a non-metallic holder) in contact with a rotating specimen held firmly in a non-metallic circular vessel which facilitated use of corrosive solutions. Details of the experimental setup have been provided in a previous publication [35]. This experimental setup forms a standard 3-electrode electrochemical corrosion cell wherein the unmasked specimen constituted a working electrode (W.E), carbon rod formed an auxiliary electrode (A.E) and a saturated silver/silver chloride (Ag/AgCl) electrode was used as a reference electrode (R.E) (all electrochemical potentials reported hereafter are with respect to this RE). Corrosive conditions were held and monitored with the help of a potentiostat (Gill AC, ACM instruments, UK). Only a small area of the sample was intentionally exposed to the rubbing action of an alumina ball and the corrosive liquid, whereas the rest of the sample was masked with the help of a non-conductive masking lacquer.

In this study a simulated body fluid (SBF) - Hank's solution (Minimum Essential Medium-Life technologies Europe B.V., The Netherlands) was used as a corrosive solution. Simultaneously

sliding wear and corrosion experiments were performed at ambient temperatures (22–24 °C) on untreated and nitrided specimens under different conditions. Namely, potentiodynamic polarisation conditions (-1 V to +1 V with a sweep rate of 45 mV min^{-1}), under open circuit potential (OCP), active dissolution potential (anodic +50 mV) and at +300 mV which appeared to promote passive layer formation on the surface (derived from the polarisation curves). Simultaneous friction coefficients were recorded as the samples were subjected to only wear (unlubricated and in open air) or combined wear-corrosion conditions.

To maintain a consistency in all experiments, a fixed linear sliding velocity of 0.1 ms^{-1} and sliding distance/time (268 m/45 min) was chosen with an intention of restricting the wear track within the nitrided zone along with a near-steady state open circuit potentials (derived from the pilot experiments for the set of experimental parameters employed in this study). A fixed normal load of 5 N (Hertzian contact pressure in the range of 1.5 GPa in static mode) was chosen for all experiments. The contact and shear stresses produced in these experiments are estimated to be similar, if not exceeding, to those experienced by a typical artificial joint under normal walking conditions [35–38], however, utilising a higher normal load also presents an opportunity of investigating the performance from a perspective of applications beyond biomedical field. Each test was repeated three times to find its repeatability and to calculate error margins derived from standard deviation of values.

2.3. Wear track and specimen characterisation

Wear mechanisms and surface artefacts were investigated with the help of Scanning Electron Microscopy (SEM) (NOVA-NANOSEM 200, FEI, The Netherlands). Secondary electron imaging mode was utilised to capture images of the virgin surfaces and the surfaces post experimentation. The working distance was 10 mm and a spot size of 3.5 was used whereas an accelerating voltage of 15–30 kV was used depending on the specimen type and image contrast requirements. The sliding wear-corrosion coefficients ($\mathbf{K_{SWC}}$) and dry sliding wear coefficients ($\mathbf{K_C}$) were calculated by profiling the cross-sectional area of the wear track with the help of a stylus profilometer (Dektak 150, Veeco Instruments, USA) with a spatial resolution of 33 nm and using a formula:

$$K_C = \frac{A_t . v}{F_N . L} \quad (1)$$

where, A_t is the cross-sectional area of the wear track (either dry or corrosive conditions) generated due to the action of mechanical wear/corrosion or both together, v is the linear velocity, F_N is the normal load in Newton (5 N here) and L is the number of laps. An Olympus BX51 M light microscope was used to capture images of the al_2O_3 counterpart. Empyrean X-ray diffractometer with Cu source (Kα, λ = 1.5418 Å) was used to conduct the XRD analysis. Glancing angle technique (θ-2θ geometry) with an incidence angle of 2° and a step size of 0.006° was used to record the diffractogram.

3. Results and discussion

In this study the HLPN of the CoCrMo alloys was carried out at −900 V. The microstructure of the untreated alloy consisted of a metastable f.c.c austenite (γ) and hcp (ϵ) phase matrix with a random distribution of metal (Co,Cr,Mo and Mn) carbides. Nitrided layers obtained consisted of a mix of equiaxed γ_N grains along with randomly distributed metal compounds ($M_{2\text{-}3}N$, M_4N, where M = Co dominated) and presence of a diffusion based Co_4N layer (white/S phase layer) at the substrate-nitrided layer interface. Total nitrided layer thickness was measured in the range of 2.83 ± 0.12 μm and had a hardness of 23 GPa. Fig. 1 shows the XRD patterns, plan view and cross-sectional SEM images of the nitrided layer which have been included to present a general overview of the materials being analysed. Readers are encouraged to read the detailed description of the microstructural characterisation and other properties (mechanical and corrosion properties) of the nitrided layer reported in our previous publications [18–20].

Tribocorrosion behaviour is very complex phenomenon wherein the degradation mechanisms of a material depend on a number of factors such as the inherent mechanical properties and corrosion resistance of the material, passivation-depassivation and repassivation kinetics, loading-unloading of the surface, role of the wear debris, supply of the reactants to the surface etc. This work focused on gaining a general understanding of nitriding effect on the tribocorrosion performance i.e., on friction coefficients, corrosion currents/potentials, and sliding wear-corrosion coefficients (K_{SWC}). In order to facilitate this, results of tests under potentiodynamic and potentiostatic polarisation conditions (OCP, anodic and passivating potentials) under rubbing and corrosion only conditions have been investigated and compared. In this work, a chemically inert al_2O_3 ball was used as the static counterpart. Under all experimental conditions (potentiodynamic, OCP and potentiostatic potentials) and for both types of specimens (untreated and treated) the alumina counterpart showed extremely low and unquantifiable wear (mainly roughening of the surface in contact-see Fig. 2). Hence, in this work, it is appropriate to focus solely on the performance of the alloy surfaces and ignore any contribution from the counterpart.

3.1. Potentiodynamic polarisation

Table 1 presents the corrosion currents/potentials measured for the nitrided and untreated specimens when tested under different corroding conditions in detail. Fig. 3a shows the results from the potentiodynamic polarisation tests in the presence and absence of sliding wear for nitrided and untreated alloy specimens. Under corrosion only conditions, nitrided samples exhibited a marked improvement in the E_{Corr} value (- 356 ± 72 mV) as compared to the untreated sample (−795 ± 16 mV) suggesting a higher resistance to corrosion. However, untreated specimen displayed a better passivating tendency and hence lower corrosion currents for a broad range of anodic potentials. This complex behaviour of the untreated specimen was attributed to the combination of Co dissolution along with an instant formation of a stable Cr_2O_3 oxide layer when the surface comes in contact with the buffer solution. This polarisation behaviour and its correlation to the microstructure has been explained in a previous publication [20].

In the case of tribocorrosive conditions, the results indicated that wear had a significant effect on the corrosion currents, and therefore on the shape of the curves. Though no significant change in the E_{Corr} value of the nitrided sample (comparing to corrosion only conditions) was observed, the untreated surface exhibited a significant rise in the E_{Corr} value.

Microstructural changes in the subsurface region (few tens of nanometer thick), especially of CoCrMo alloys, due to wear/dynamic mechanical loading of mechanical contacts under loading/wearing conditions has been well documented by various researchers [6,39]. A small nobler shift in E_{Corr} value of CoCrMo alloy following (post mechanical processing) was also reported by Namus et al. [6]. The authors attributed this change to the intentionally induced transformation of micro sized grains to nanocrystalline sizes. On other hand, the same microstructural changes were attributed for the drop in corrosion resistance when the specimens were subjected to tribocorrosive conditions. In this

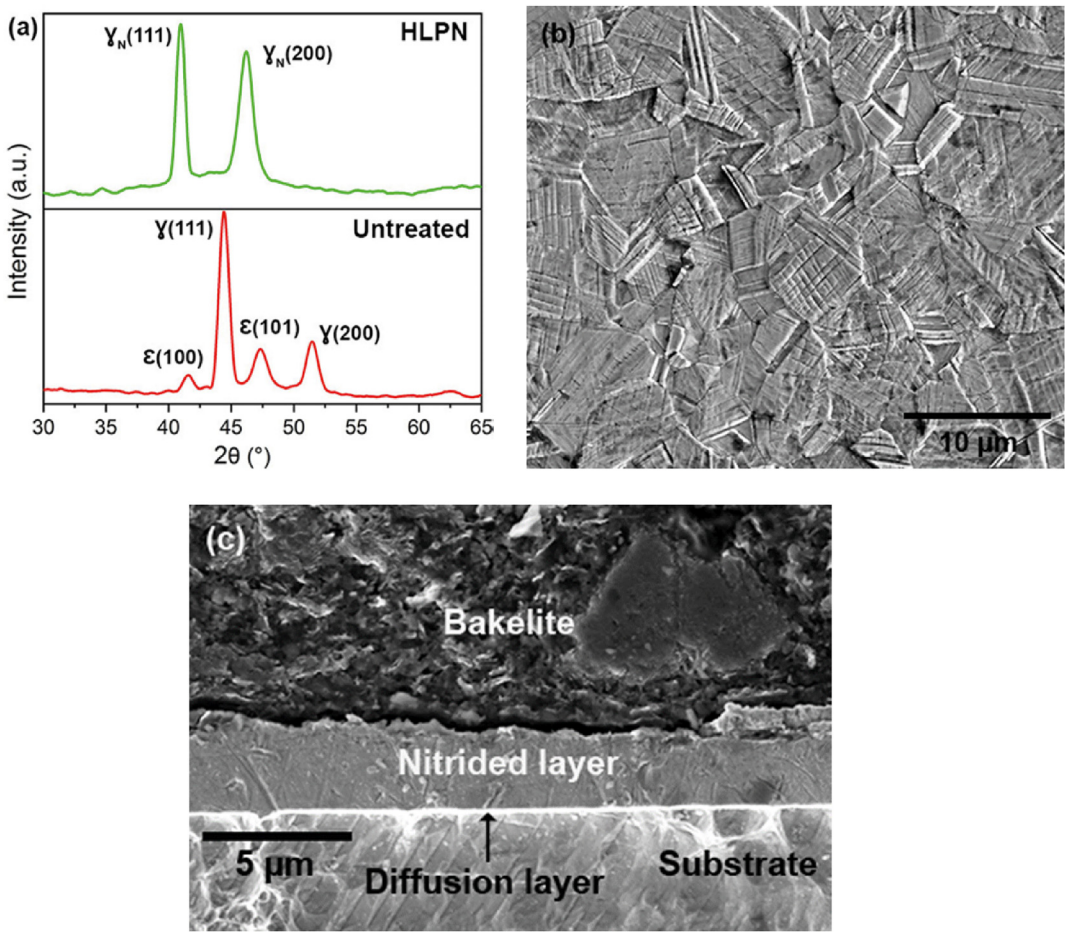

Fig. 1. Microstructure studies of the HLPN treated CoCrMo alloy (a) XRD results (b) nitrided surface in plan view (c) cross-sectional view.

study, the normal load of 5 N (Hertzian contact pressure in the range of 1.5 GPa) is well suited to make these microstructural changes on a subsurface level in untreated CoCrMo alloys [6]. Also, as anticipated, removal of passive layers (predominantly Cr_2O_3) and providing fresh surfaces due to a constant rubbing action leads to a higher corrosion current in most anodic and passivating potentials (up to +600 mV). This could well explain the increment in E_{Corr} value and corrosion currents observed for the untreated alloy.

On the contrary, the nitrided layer exhibited almost similar E_{Corr} values for both tribocorrosive and corrosion only conditions and significantly lower anodic and passive current values than untreated alloys under tribocorrosive conditions. Thus, there is enough primary evidence to suggest that under the current set of experimental parameters (normal load of 5 N and sliding distance in the range of approximately 268 m), the nitrided layer does not experience any microstructural changes induced through mechanical action (load or wearing conditions). This corresponds well with the reports of improved surface mechanical properties observed when nitrided using HLPN process. These nitrided specimens showed a significant increase in hardness (from 8 to 22 GPa), fracture toughness (K_{Ic}) (from 906.9 to 872.9 MPa $mm^{1/2}$) and impact load fatigue resistance as compared to untreated CoCrMo alloys [19]. These results are interesting and warrant further studies to confirm the benefits of nitriding on the microstructure stability under sliding wear-corrosion conditions.

The friction and wear performance of unlubricated (dry) sliding wear of untreated and nitrided F75 alloy specimens was thoroughly analysed in a previous publication [21] which demonstrated the influence of superior nitrided microstructure on friction coefficient and wear resistance offered by the nitrided surfaces. In dry conditions (and similar normal load of 5 N and a sliding distance in the range of >0.5 km), the fluctuation in friction coefficient value of the untreated alloy was attributed to a complex interaction between the static counterpart and the broken/pulverised asperity contacts along with the compacted oxidised wear debris (tribolayer) formed in the alloy surface wear track. The wear debris generated was found to be influenced by the mechanically weak asperities and the wear mechanism was found to be mainly 2 body and 3 body contact abrasion. In the case of the nitrided alloy, the wear mechanism was found to be dominated by oxidative wear amid a small contribution from 2/3 body abrasion. The synergy between high hardness and enhanced ductility of the underlying nitride layer resulted in high wear resistance and lower wear debris generation which was found to be nanoscale in size mostly generated by micro-cutting of the asperities.

However, under sliding wear corrosion conditions, similar to those employed in this study, aqueous environment will play a significant role. It will impart a lubricating effect and also facilitate the formation of hydrated oxides (corrosion products) instead of the oxidative tribolayers formed due to high flash temperatures in dry conditions. Also, due to design of the experimental setup which consisted of a rotating action of the test cell and hence of the corrosive solution, any loose wear debris generated will be effectively carried away from the wear track. This will have a clear influence on the μ values. Fig. 3b shows the effect of electrochemical potentials on the friction coefficient (μ) values. As anticipated, irrespective of

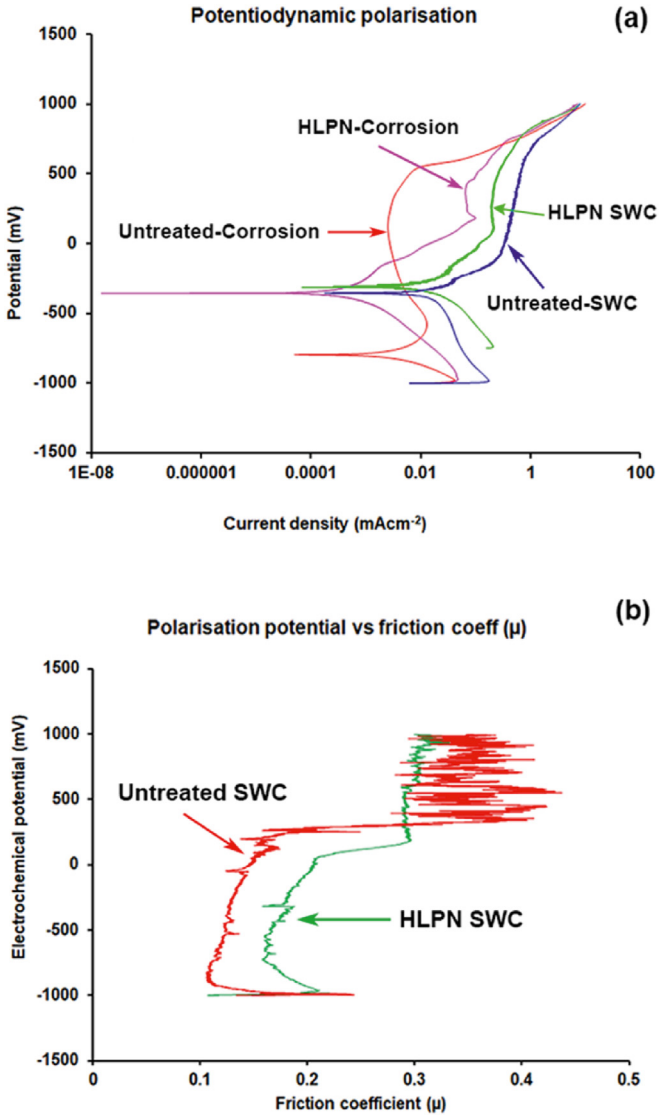

Fig. 2. Sliding wear corrosion results (a) Potentiodynamic polarisation curves recorded (b) corresponding friction coefficient values as a function of electrochemical potentials.

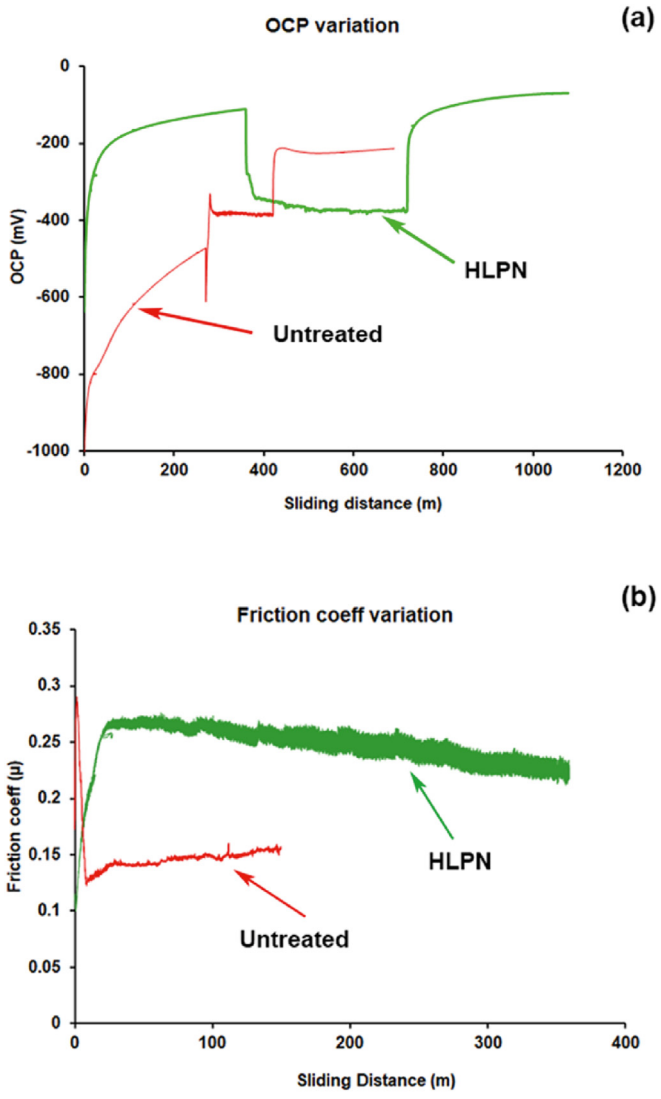

Fig. 3. (a) Variation in OCP (b) corresponding friction coefficient values recorded.

the electrochemical potential, the μ values were lower for both specimens as compared to the dry sliding μ values (0.47, see Table 2) when tested for an identical sliding distance and normal load. This can be attributed to the limited lubricating effect of the aqueous solution used in these experiments.

Under cathodic potentials (no corrosion), the untreated alloys exhibited lower μ values than the nitrided alloys. The lower surface roughness of the polished untreated alloy (Ra = 13 nm) along with the mechanically weak asperities which plastically deform easily and a cushioning effect of instantaneously forming passive layer(s) [23] could be attributed for the lower value of μ recorded. In the case of nitrided alloy, the hard but comparatively rougher surface (Ra = 65 nm) seemed to delay the generation of wear debris as well as negate the lubricating effect of the aqueous solution.

On the onset of corrosion, a marked rise in μ was observed for both specimens. Rapid dissolution of the surface, formation of new asperities resulting to increased roughness as well as facilitation of 2/3 body abrasion could be responsible for the sharp rise in μ values

Table 1
Electrochemical potentials and corrosion currents measured for nitrided and untreated specimens.

Specimen	Experimental Condition	Electrochemical potential -Rubbing (mV)	Corrosion current pre rubbing ($mA.cm^{-2}$)	Rubbing corrosion current ($mA.cm^{-2}$)	Corrosion current post rubbing ($mA.cm^{-2}$)
HLPN	**OCP**	−366.49 ± 2.7			
	Anodic (+50 mV)		$1.9 \pm 2.3 \times 10^{-2}$	$7.3 \pm 2.1 \times 10^{-2}$	$1.1 \pm 1.1 \times 10^{-2}$
	Passive (+300 mV)		$7.5 \pm 1.1 \times 10^{-3}$	$2.7 \pm 1.3 \times 10^{-1}$	$3.1 \pm 0.7 \times 10^{-3}$
Untreated	**OCP**	−381.46 ± 4.9			
	Anodic (+50 mV)		$1.0 \pm 1.3 \times 10^{-3}$	$2.5 \pm 0.4 \times 10^{-1}$	$3.1 \pm 1.5 \times 10^{-4}$
	Passive (+300 mV)		$3.2 \pm 1.2 \times 10^{-3}$	$3.0 \pm 0.7 \times 10^{-1}$	$5.9 \pm 4.2 \times 10^{-4}$

Table 2
Friction coefficients measured under different environmental conditions.

Specimen	Environmental Condition	Steady state Friction coefficient (μ)
HLPN treated	**Air**	0.47 ± 0.05
	OCP	0.26 ± 0.05
	Anodic (+50 mV)	0.30 ± 0.01
	Passive (+300 mV)	0.32 ± 0.01
Untreated	**Air**	0.47 ± 0.06
	OCP	0.15 ± 0.01
	Anodic (+50 mV)	0.35 ± 0.01
	Passive (+300 mV)	0.35 ± 0.01

in these potentials. In the passivating potentials, the friction coefficient curve of the untreated alloy appeared very noisier. The μ values vigorously fluctuated between 0.3 and 0.55. On the contrary, nitrided specimens' friction curves appeared relatively smoother and recorded a near steady μ value around 0.3 which was lower than the untreated specimen. The benefit of nitriding was clear in passivating conditions. Results indicate that nitrided layer not only maintained its structural integrity with a superior wear resistance, but also produced a well adhered continuous passive layer which was ably supported by the underneath hard and wear resistant nitride layer. Table 2 displays the friction coefficient values recorded for the nitrided and the untreated specimens under different environmental conditions.

3.2. Open circuit potentials (OCP)

Fig. 4a shows the variation in OCP values and the corresponding friction coefficient as a function of sliding wear. As anticipated, in the absence of sliding wear, the OCP values recorded for the nitrided specimens (−175 ± 54 mV) were higher and stabilised quickly as compared to the untreated specimens (−532 ± 89 mV). In the case of nitrided specimen, the OCP variation observed was typical for passive metals where in the rubbing action leads to the removal of passive layers and exposure of fresh surface and hence a drop in the electrochemical potential [36,40]. As soon as the rubbing action was stopped, the electrochemical potentials returned to the pre-rubbing values.

In the case of untreated specimens, the behaviour appeared to be complex wherein a drastic drop in the OCP value was observed at the initiation of the rubbing action of the ball. However, it quickly recovered and surpassed the OCP value recorded in the absence of wear to reach a slightly nobler value (sub-peak) further followed by a drop eventually to stabilise to a value (−381 ± 5 mV) until the specimens were subjected to the rubbing action of the counterpart alumina ball. CoCrMo alloy (F75) has a strong tendency to passivate spontaneously [20,23] (also evident from the polarisation experiments) when it comes in contact with the SBF. Accordingly, it showed an initial sharp rise in the OCP value as soon as the rubbing action exposed a fresh surface (amid increasing wear track dimensions) to the SBF. This complex behaviour was a resultant of a mixture of competitive process of passivation, mechanical removal and repassivation of the surface along with any galvanic coupling effects [2] for the untreated alloy under the dynamic rubbing conditions until it reached an equilibrium [41]. Even though the untreated alloy spontaneously passivated, its low hardness and high wear rate facilitated removal of material and generation of fresh surfaces along with the easy removal of passive protection under the rubbing action of the ball. Thus, its steady state OCP value under rubbing resulted to be more electrochemically negative (−381 ± 5 mV) as compared to the nitrided surfaces (−366 ± 2.7 mV).

As soon as the rubbing action was halted, the OCP climbed to a nobler value (- 215 ± 5 mV) and remained steady until the end of the test. The increment in OCP value post rubbing further strengthens the argument of microstructural changes in the untreated subsurface regions underneath the wear track induced due to the mechanical loading (see section 3.1).

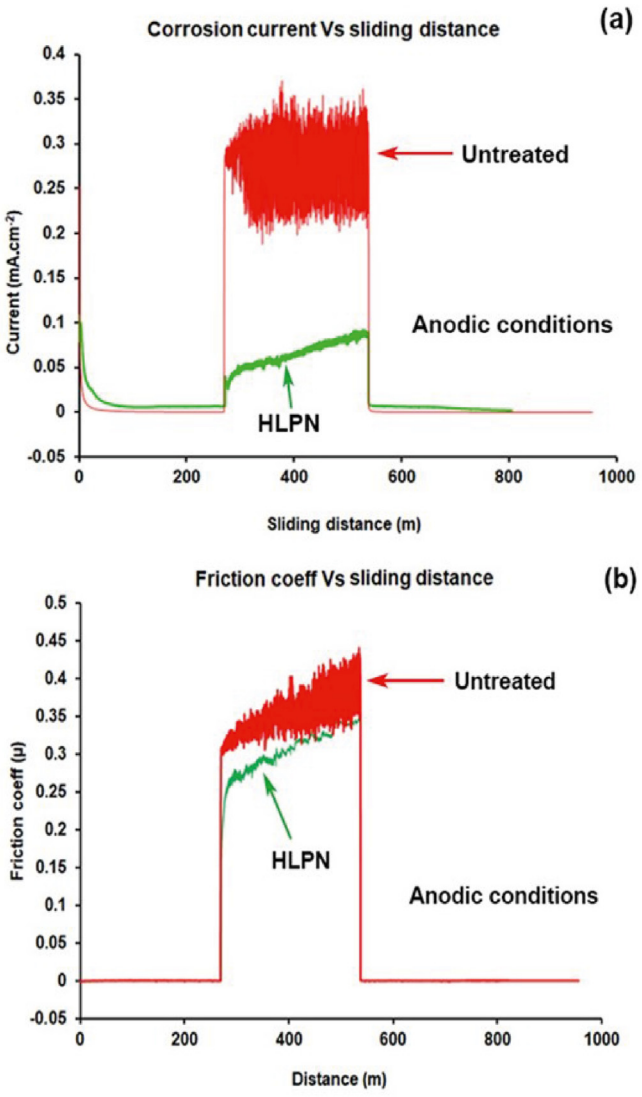

Fig. 4. Sliding wear corrosion results in anodic conditions (a) Variation in corrosion current (b) corresponding friction coefficient values recorded.

Corresponding friction coefficient behaviour (μ) can be observed in Fig. 3b and Table 2. The nitrided specimens, owing to its relatively high roughness (65 nm) and its ability to retain its structural integrity exhibits a higher friction coefficient value ($\mu = 0.26 \pm 0.05$) as compared to the untreated specimen ($\mu = 0.15 \pm 0.01$) and is consistent with results found in the literature for tribocorrosion studies of nitrided CoCrMo alloys [30,32,33]. Consequently, the sliding wear corrosion coefficient (K_{SWC}) for the nitrided specimen was marginally higher (in the range of 6.52×10^{-15}) as compared to the untreated specimen (in the range of 3.92×10^{-15}); Fig. 5. Lower friction coefficients in the case of untreated specimens could also be attributed to the lubricating effect of the less adhered corrosion products (inherent passive layers) formed in the wear track.

3.3. Anodic potentials

Fig. 6 shows the results obtained when the specimens were subjected to sliding wear corrosion experiments under anodic

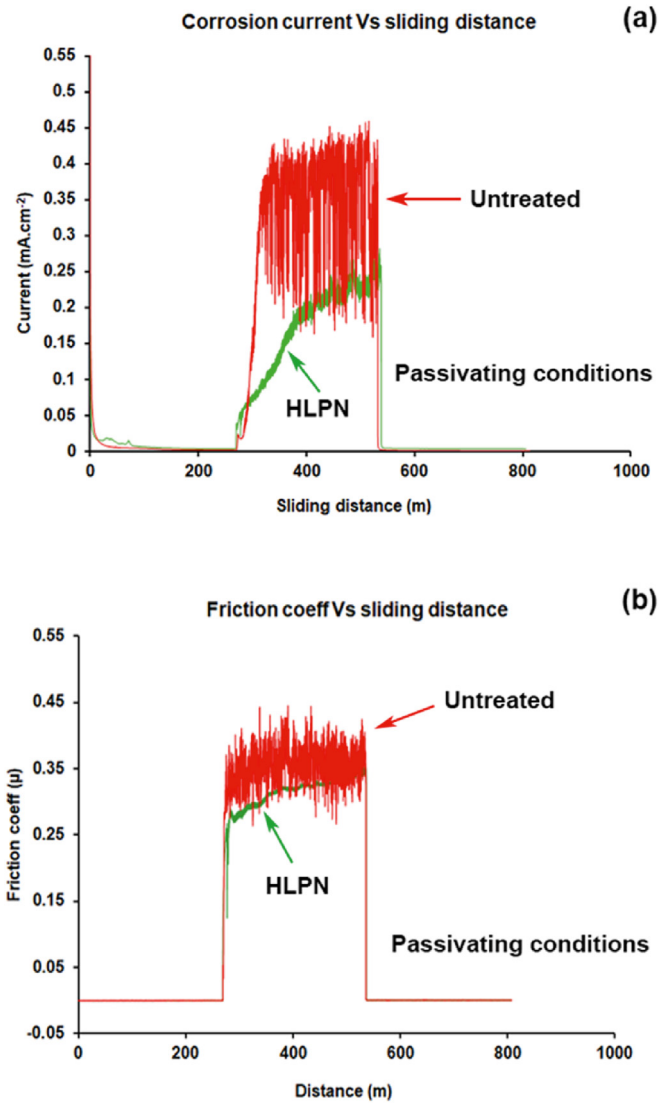

Fig. 5. Sliding wear corrosion results in passivating conditions (a) Variation in corrosion current (b) corresponding friction coefficient values recorded.

dissolution potentials of +50 mV (see Fig. 3a). The beneficial effect of nitriding on the microstructure and eventually on the tribo-corrosion behaviour was clear. Both, corrosion currents (during rubbing) and the friction coefficient of the nitrided samples were lower as compared to those observed for the untreated specimen. This is significant, since the corrosion current of the untreated specimen when the specimens were submerged in the solution were an order of magnitude lower (because of the instantaneous passivation of the surface) before the initiation of the rubbing action. The friction coefficient of the untreated specimen exhibited severe fluctuations in the values suggesting an extreme and dynamic surface wear/deformation and dissolution, rapid depassivation/passivation phenomenon vigorously and concurrently taking place in the wear track. Also, as K_{SWC} values presented in Fig. 5 suggested, deeper wear tracks formed in the untreated specimens may have resulted in a larger contact area between the ball and specimen giving rise to a higher roughness, higher corrosion current and eventually higher friction coefficients [32].

In comparison, friction coefficient of the nitrided specimen was much smoother and significantly lower, which benefited from a superior microstructure (high hardness, fracture toughness (K_{Ic}) and impact load fatigue resistance) which was resilient to corrosion. Consequently, a significant difference in the K_{SWC} was observed. Nitrided specimens exhibited a K_{SWC} value (6.14×10^{-15}) which was an order of magnitude lower compared to the untreated specimen (3.4×10^{-14}) as presented in Fig. 5. The severe fluctuation in μ suggested that the corrosion products dislodged from the surface of the untreated specimen could have led to an increment in 2/3 body contact abrasion mechanism (mechanical component) and its contribution in the total wear loss measured.

3.4. Passivating potentials

Fig. 7 shows the results obtained when the specimens were subjected to sliding wear corrosion experiments under passivating potentials of +300 mV (see Fig. 3a). The corrosion current and sliding wear friction behaviour (mean values and general trend) for the untreated specimen observed at these potentiostatic potentials were found to be similar to those observed for the dissolution potentials. Consequently, the K_{SWC} value were also almost identical (6.41×10^{-15}). On closer inspection (Fig. 7), both μ and corrosion current showed abrupt and large fluctuations in their nature. Even though the bare alloy has a stronger passivating tendency, under sliding wear conditions, the nature of the passive layers and a softer base meant material was easily removed thereby facilitating increased contact between the ball and specimen as wear progressed resulting in higher fluctuations in μ and corrosion current values.

In comparison to anodic potentials, the nitrided specimen exhibited a slight drop in the friction coefficient and consequently a slight drop in the K_{SWC} value (4.29×10^{-15}). Similar to anodic potentials, it was an order of magnitude lower to the untreated specimens in similar testing conditions (Fig. 5). This can be attributed to a combination of factors. Firstly, a drop in the wear-corrosion synergism resulting to a drop in the total material removal rate (mechanical component due to a hard microstructure). Secondly, drop in the corrosion rate contribution due to the corrosion resistant microstructure consisting of S phase diffusion layer and the top compound layer. Thirdly, some lubricating effect of a rapidly growing passive oxide layer effectively supported by the mechanically strong nitride layer underneath since diffused nitrogen has been shown to promote growth of stable oxide films [23].

3.5. Wear scar analysis and material removal mechanisms

Figs. 8–10 show the wear tracks generated under different corroding conditions. Irrespective of an electrochemical potential applied, both untreated and treated specimens exhibited ploughing groves which were mostly parallel to each other, albeit with varying degree of roughness and micro-cutting. Since the experimental setup consisted of rotating the corrosion cell, any loose wear debris generated due to the sliding wear action or corrosion was efficiently washed away from the wear track, reducing the probability and amount of 3-body rolling abrasion. To some extent wear debris was also found adhered to the rough areas of the alumina counterpart (Fig. 2). The SEM images strongly suggest that 2 body abrasion appeared to be the dominant mechanical wear mechanism. Under OCP conditions, untreated specimens also exhibited some pitting corrosion and grain pull-out possibly exacerbated due to corrosion, Fig. 8d.

In general, wear tracks generated on nitrited specimens and under the passivating potentials appeared smoother and with shallower groves as compared to the wear tracks in OCP and anodic conditions. In passivating conditions, there is a possibility that the instanteneously growing oxide films can reduce the contact between the counterpart and the specimen surface offering

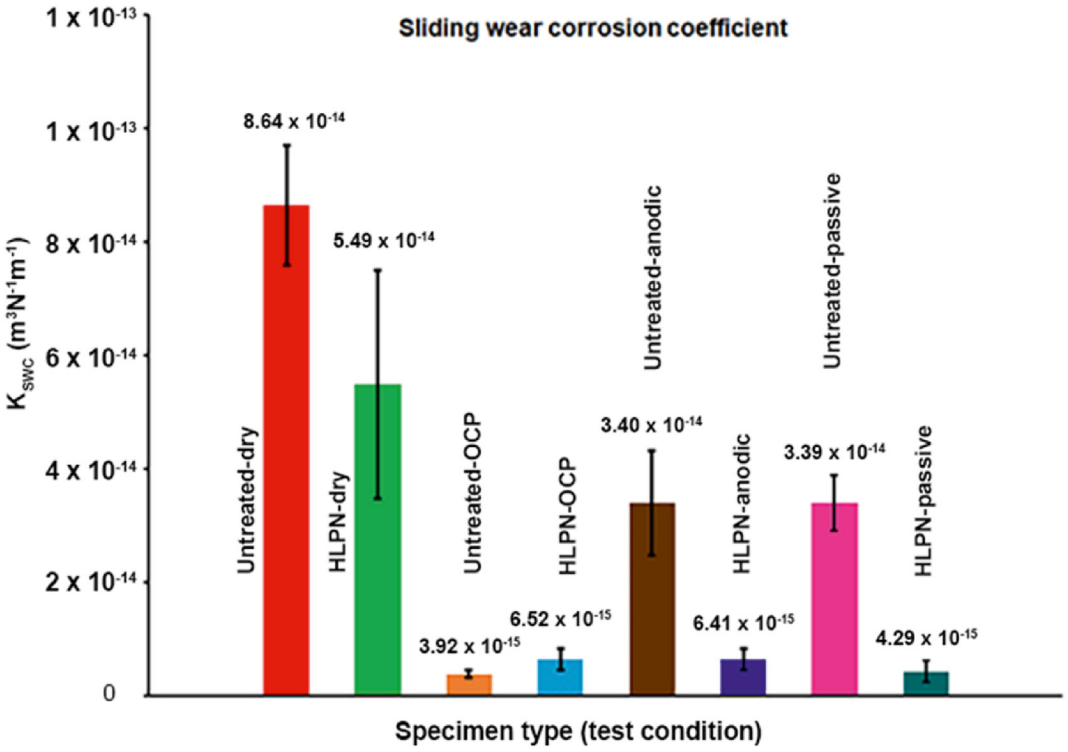

Fig. 6. Sliding Wear Corrosion coefficients (KSWC) calculated for the nitrided and untreated specimens under various environmental conditions.

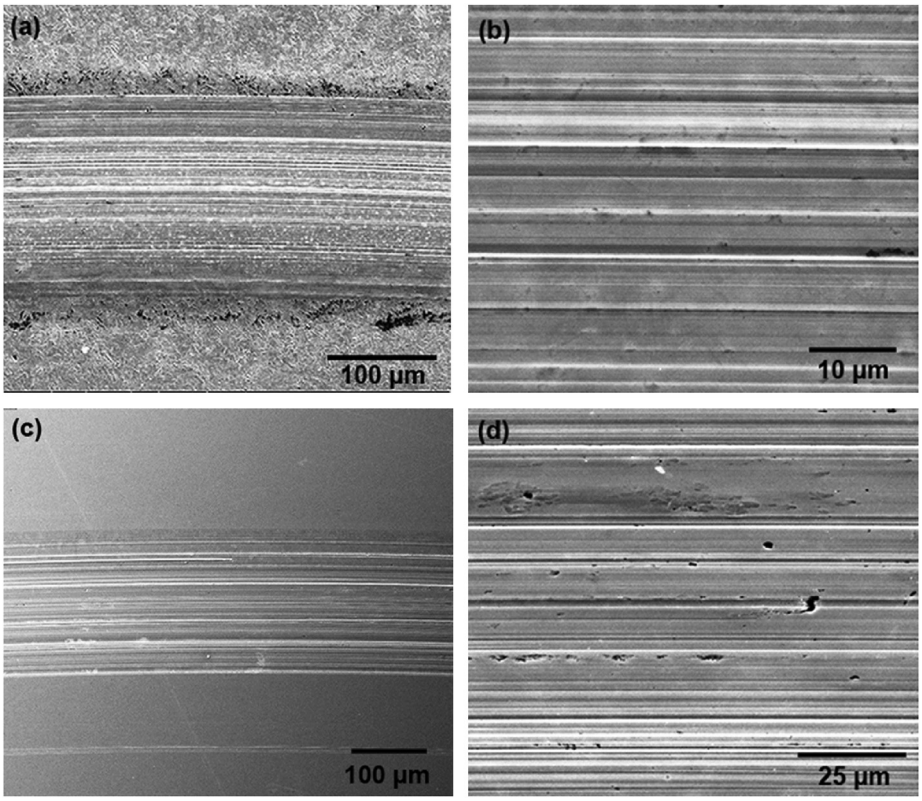

Fig. 7. SEM images of wear track generated under OCP conditions: (a) HLPN-low magnification (b) HLPN-high magnification (c) untreated -low magnification (d) untreated- high magnification.

protection to some extent (depending on the type and nature of the oxide(s) formed and their adherence or easly removal from and by the surfaces in contact) before being dislodged and flushed away by the fluid [42]. In anodic dissolution conditions, the wear track will be depleted of this protection. On the contrary, dissolution of the microstructure could roughen the surface leading to higher friction

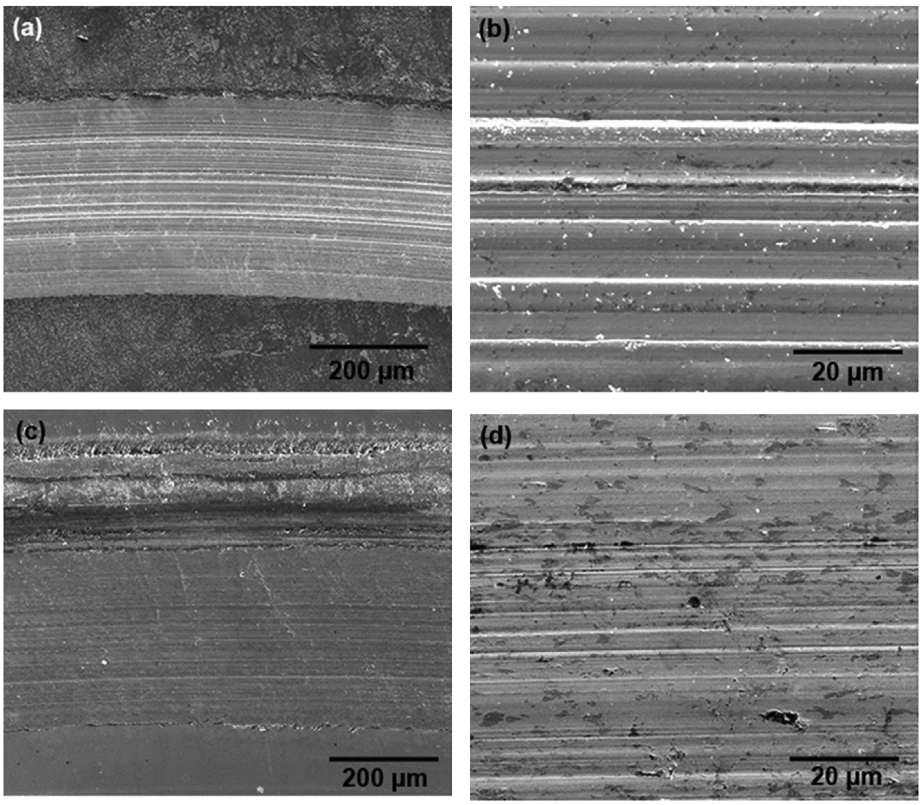

Fig. 8. SEM images of wear track generated under anodic conditions: (a) HLPN-low magnification (b) HLPN-high magnification (c) untreated -low magnification (d) untreated- high magnification.

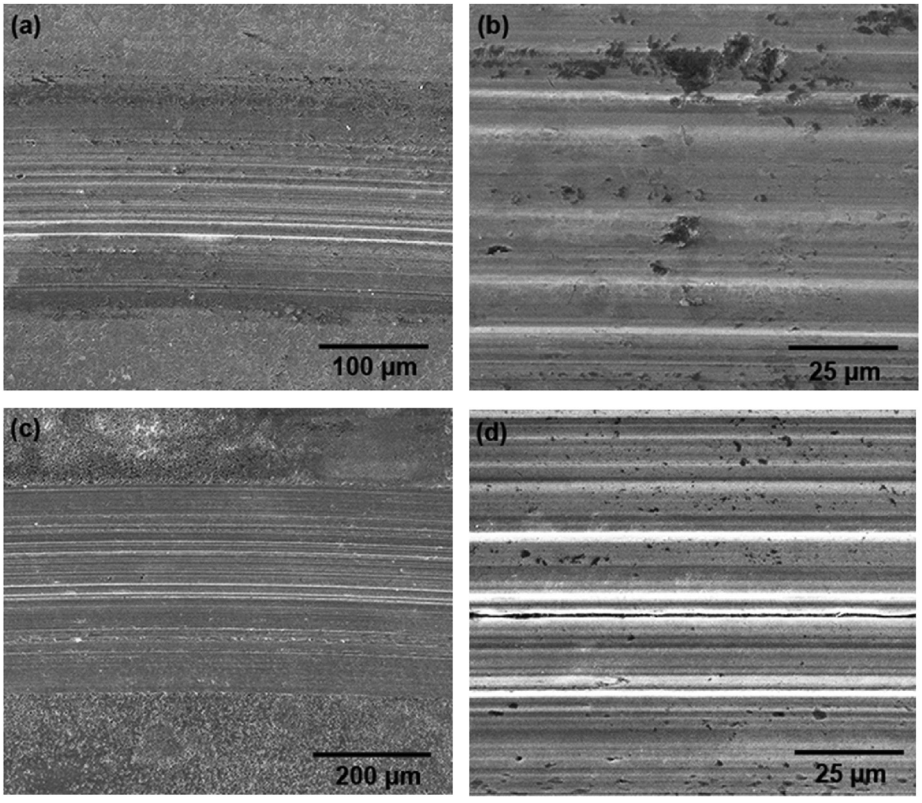

Fig. 9. SEM images of wear track generated under passivating conditions: (a) HLPN-low magnification (b) HLPN-high magnification (c) untreated -low magnification (d) untreated-high magnification.

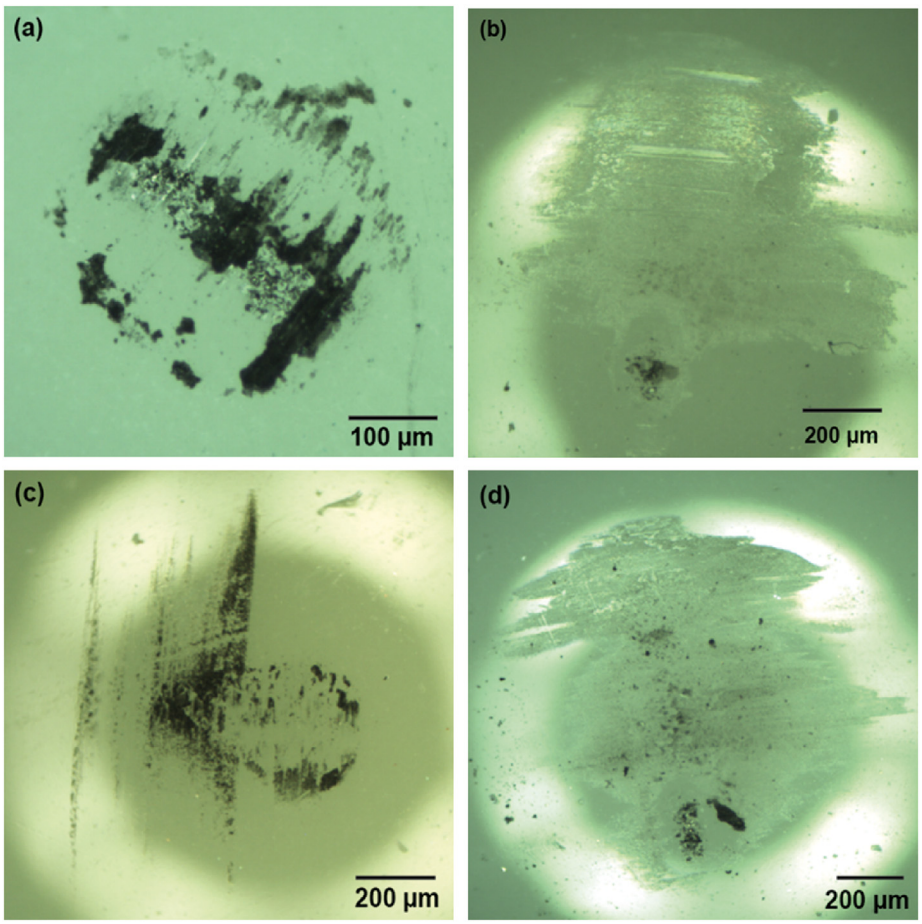

Fig. 10. Light microscope images (dark field mode) of the scars generated on al2O3 counterpart at end of tests: (a) untreated- anodic potential (b) HLPN-anodic potential (c) untreated -passive potentials (d) HLPN- passive potentials.

coefficient and eventually higher wear rate leading to deeper groves as observed in the SEM images and evident from the higher Kswc values (Fig. 5). In the case of OCP conditions, the areas which are not under the sliding contact can instantenously repassivate [42] and thus can offer limited protection to the specimen underneath resulting in smoother and shallower grooves as compared to the anodising conditions leading to a lower Kswc as compared to anodising conditions.

In case of a like to like comparison, abrasion groves in the wear tracks on nitrided specimens appeared shallower than the untreated specimens at respective potentials. In general, ploughing due to 2 body abrasion appeared to be the dominating wear mechanism for both types of specimens, with no evidence of macroscale material flaking or removal mainly due to corrosion. No evidence of any material transfer from the alumina counterpart or adherence of the wear debris within the wear track (due to the pressing action of the counterpart on successive passes) was evident when observed under SEM or optical microscopy. Only adherence of some wear debris on the roughened alumina counterpart (Fig. 2) was found.

The microstructure of the untreated CoCrMo alloy consisted of randomly distributed metal carbides (CoC, CrC, MoC and MnC) in a matrix of a metastable f.c.c autenite (γ) and h.c.p (ϵ) phases (Fig. 1a) [20]. The bare alloy exhibited a clear passivating tendency (approximately above potentials of −600 mV under corrosion only and −30 mV for SWC conditions) when electrochemically polarised in Hank's solution (Fig. 3a). There is a general consensus in the liturature that passivity of CrCoMo alloys is achieved mainly through the formation of oxides of Cr (Cr_2O_3) which is readily available from the matrix and to some extent through Mo based oxides. However, Co readily dissolves as soon as it comes in contact with Hank's solution and continues to dissolve even when passive layers are formed [43]. Thus as a material removal mechanism, under anodic sliding wear conditions, the hard ceramic ball can be visualised to plough through very thin passive layers (Cr and Mo based) and underneath soft bulk alloy and dislodged material mainly by 2 body abrasion mechanism abily assisted by preferential dissolution of the γ and ϵ phases (galvanic pairing with relatively noble metallic carbides) [20] and leaching of Co from the matrix. This led to a higher fricion coefficient, mainly due to the roughening of the matrix caused by the protruding carbides and dissolved matrix [20] along with the widening wear track leading to an increasing contact between the ball and the specimen as the wear progressed. Eventually these conditions resulted in a higher synergy between wear and corrosion and can be attributed for the higher K_{SWC} values observed in the results provided in Fig. 5. Even though grain refinement in the plastically deformed subsurface layers of the wear track had a significant impact in improving the E_{Corr} value of the untreated alloy, it exhibited a negligible influence in reducing this synergy. Under passivating conditions, these order of events were expected to be similar amid through varying degree of passive layer thickness and corrosion contributions.

The microstructure of the HLPN nitrided specimens consisted of a distinct Co_4N white layer, also called as a S phase layer (around 283 nm thick), at the bulk alloy-nitrided layer interface and approximately a 2.5 μm thick top layer consisting of metal

compounds ($M_{2\text{-}3}N$ and M_4N) where M was mainly Co mainly made up of expanded austenite (γ_N) grains and some ε_N grains (Fig. 3a and c) [20]. The conditions of HLPN process employed for these set of samples (−900 V bias) were just adequate to energise and diffuse enough nitrogen ions to form a solid solution (f.c.c) of expanded austenite (γ_N) without the formation of CrN phase which has been reported to form at a higher dose of diffused nitrogen [31] and attributed for the redcution of corrosion resistance in nitrided CoCrMo alloys [30–32]. Thus the combination of high mechanical properties (high hardness, high fatigue and impact toughness [19]) and high corrosion resistance (reduction in Co as well as Cr and Mo dissolution [44] and stabilisation of passive layers [30]) led to lower wear component (mechanical), lower corrosion and a lower synergy between wear and corrosion. Apparently, 2 body abrasion was also found to be the dominant mechanical material removal mechanism for the nitrided alloy. In anodic conditions, it was assisted by preferential dissolution of ε_N grains [20] amid a significant reduction in the corrosion of the alloy evident from the low corrosion currents (Table 1) since the hard less wearing nitride layer delayed the widening of the weartrack and exposure of fresh surface. In passive conditions, the stable passive layer appeared to be ably supported by the hard niride layer thereby reducing the K_{SWC} values.

4. Conclusions

The tribocorrosion performance of a medical grade F75 alloy (CoCrMo alloy) nitrided with the HIPIMS Low-Pressure Nitriding (HLPN) technique was successfully analysed. In general, the results indicated that the tribocorrosion resistance of the alloy had a strong dependency on the microstructure as well as on the corroding conditions altered by varying the electrochemical potentials applied to the system. From the current studies, the following conclusions could be derived. Nitriding had a beneficial effect on the corrosion performance of the F75 alloys. Under corrosion only conditions, nitrided surfaces had nobler E_{Corr} values as compared to untreated surfaces. Under potentiodynamic sliding-wear corrosive conditions the E_{Corr} values of the untreated alloy nearly matched with those of the nitrided alloy. This enhancement of E_{Corr} value could be attributed to the microstructural changes instigated by wear in the subsurface regions. However, barring this positive effect, untreated specimens recorded higher corrosion currents under all anodic as well as passivating potentials. In contrast, nitrided specimens exhibited lower friction coefficient values and corrosion currents under anodic and passivating potentials as compared to the untreated alloy. Near similar E_{Corr} values observed in the absence and presence of sliding wear suggest that the nitrided microstructure is resilient to microstructural changes instigated by wear. Consequently, owing to better wear and corrosion resistance, nitrided specimens exhibited lower sliding wear coefficient (K_{SWC}) values in anodic and passivating conditions which was an order of magnitude lower than those calculated for the untreated specimens. HIPIMS nitriding technique provided a suitable way to enhance tribocorrosion resistance of CoCrMo alloys by promoting growth of nitrided microstructure which retained high hardness, toughness and corrosion resistance under tribocorrosive conditions employed in this study.

Declaration of competing interest

The authors declare the following financial interests/personal relationships which may be considered as potential competing interests: Krishnananda Shukla reports financial support was provided by Zimmer Biomet.

Acknowledgement

Authors would like to acknowledge Zimmer-Biomet, UK for providing financial support to carryout doctoral research of one of the authors, Krishnanand Shukla.

References

[1] M. Navarro, A. Michiardi, O. Castaño, J.A. Planell, Biomaterials in orthopaedics, J. R. Soc. Interface 5 (27) (2008) 1137–1158.
[2] N. Espallargas, C. Torres, A.I. Muñoz, A metal ion release study of CoCrMo exposed to corrosion and tribocorrosion conditions in simulated body fluids, Wear 332–333 (2015) 669–678.
[3] B. Stojanović, C. Bauer, C. Stotter, T. Klestil, S. Nehrer, F. Franek, M. Rodríguez Ripoll, Tribocorrosion of a CoCrMo alloy sliding against articular cartilage and the impact of metal ion release on chondrocytes, Acta Biomater. 94 (2019) 597–609.
[4] D.M. Vasconcelos, S.G. Santos, M. Lamghari, M.A. Barbosa, The two faces of metal ions: from implants rejection to tissue repair/regeneration, Biomaterials 84 (2016) 262–275.
[5] C. Valero-Vidal, L. Casabán-Julián, I. Herraiz-Cardona, A. Igual-Muñoz, Influence of carbides and microstructure of CoCrMo alloys on their metallic dissolution resistance, Mater. Sci. Eng. C 33 (8) (2013) 4667–4676.
[6] R. Namus, W.M. Rainforth, Y. Huang, T.G. Langdon, Effect of grain size and crystallographic structure on the corrosion and tribocorrosion behaviour of a CoCrMo biomedical grade alloy in simulated body fluid, Wear 478–479 (2021), 203884.
[7] A. Fischer, S. Weiß, M.A. Wimmer, The tribological difference between biomedical steels and CoCrMo-alloys, J. Mech. Behav. Biomed. Mater. 9 (2012) 50–62.
[8] R. Wei, T. Booker, C. Rincon, J. Arps, High-intensity plasma ion nitriding of orthopedic materials: Part I. Tribological study, Surf. Coat. Technol. 186 (1) (2004) 305–313.
[9] A. Çelik, Ö. Bayrak, A. Alsaran, İ. Kaymaz, A.F. Yetim, Effects of plasma nitriding on mechanical and tribological properties of CoCrMo alloy, Surf. Coat. Technol. 202 (11) (2008) 2433–2438.
[10] D.C. Ba, L. Xu, Q. Wang, Effects of plasma nitriding ion beam flux density and time on the properties of CoCrMo alloy, Vacuum 119 (2015) 214–222.
[11] Q. Wang, C. Huang, L. Zhang, Microstructure and tribological properties of plasma nitriding cast CoCrMo alloy, J. Mater. Sci. Technol. 28 (1) (2012) 60–66.
[12] G. Dearnaley, J.H. Arps, Biomedical applications of diamond-like carbon (DLC) coatings: a review, Surf. Coat. Technol. 200 (7) (2005) 2518–2524.
[13] C. Skjöldebrand, J.L. Tipper, P. Hatto, M. Bryant, R.M. Hall, C. Persson, Current status and future potential of wear-resistant coatings and articulating surfaces for hip and knee implants, Mater, Today Bio 15 (2022), 100270.
[14] P.E. Hovsepian, A.P. Ehiasarian, Y. Purandare, A.A. Sugumaran, T. Marriott, I. Khan, Development of superlattice CrN/NbN coatings for joint replacements deposited by high power impulse magnetron sputtering, J. Mater. Sci. Mater. Med. 27 (9) (2016) 147.
[15] P.E. Hovsepian, A.A. Sugumaran, M. Rainforth, J. Qi, I. Khan, A.P. Ehiasarian, Microstructure and load bearing capacity of TiN/NbN superlattice coatings deposited on medical grade CoCrMo alloy by HIPIMS, J. Mech. Behav. Biomed. Mater. 132 (2022), 105267.
[16] A.P. Ehiasarian, Fundamentals and Applications of HIPIMS, Research Signpost, India, 2007, pp. 35–86.
[17] A.A. Ehiasarian, P. Hovsepian, Plasma Nitriding by HIPIMS Discharge, Sheffield Hallam University Technical Report, 2005.
[18] K. Shukla, A.A. Sugumaran, I. Khan, A.P. Ehiasarian, P.E. Hovsepian, Low pressure plasma nitrided CoCrMo alloy utilising HIPIMS discharge for biomedical applications, J. Mech. Behav. Biomed. Mater. 111 (2020), 104004.
[19] K. Shukla, Y.P. Purandare, I. Khan, A.P. Ehiasarian, P.E.H. Hovsepian, Effect of nitriding voltage on the impact load fatigue and fracture toughness behaviour of CoCrMo alloy nitrided utilising a HIPIMS discharge, Surf. Coat. Technol. 400 (2020), 126227.
[20] K. Shukla, Y. Purandare, A. Sugumaran, A. Ehiasarian, I. Khan, P. Hovsepian, Correlation between the microstructure and corrosion performance of the HIPIMS nitrided bio-grade CoCrMo alloy, J. Alloys Compd. 879 (2021), 160429.
[21] A.A. Sugumaran, K. Shukla, I. Khan, A.P. Ehiasarian, P.E. Hovsepian, Dry sliding wear mechanisms of HIPIMS plasma nitrided CoCrMo alloy for medical implant applications, Vacuum 185 (2021), 109994.
[22] P. Hovsepian, K. Shukla, A. Sugumaran, Y. Purandare, I. Khan, A. Ehiasarian, A novel plasma nitriding process utilising HIPIMS discharge for enhanced tribological and barrier properties of medical grade alloy surfaces, Mater. Lett. 313 (2022), 131782.
[23] H. Dong, S-phase surface engineering of Fe-Cr, Co-Cr and Ni-Cr alloys, Int. Mater. Rev. 55 (2) (2010) 65–98.
[24] A. Bazzoni, S. Mischler, N. Espallargas, Tribocorrosion of pulsed plasma-nitrided CoCrMo implant alloy, Tribol. Lett. 49 (1) (2013) 157–167.
[25] J. Lutz, C. Díaz, J.A. García, C. Blawert, S. Mändl, Corrosion behaviour of medical CoCr alloy after nitrogen plasma immersion ion implantation, Surf. Coat. Technol. 205 (8) (2011) 3043–3049.

[26] Y. Liu, B. Chen, Vivo corrosion of CoCrMo alloy and biological responses: a review Mater, Technol. 33 (2) (2018) 127–134.
[27] M.M. Stack, Mapping tribo-corrosion processes in dry and in aqueous conditions: some new directions for the new millennium, Tribol. Int. 35 (10) (2002) 681–689.
[28] S. Mischler, A.I. Munoz, Tribocorrosion, Elsevier, Oxford, 2018, pp. 504–514.
[29] D. Sun, J.A. Wharton, R.J.K. Wood, Effects of proteins and pH on tribocorrosion performance of cast CoCrMo – a combined electrochemical and tribological study, Tribol. Mater. Surface Interfac. 2 (3) (2008) 150–160.
[30] J. Lutz, S. Mändl, Reduced tribocorrosion of CoCr alloys in simulated body fluid after nitrogen insertion, Surf. Coat. Technol. 204 (18) (2010) 3043–3046.
[31] Z. Guo, X. Pang, Y. Yan, K. Gao, A.A. Volinsky, T. Zhang, CoCrMo alloy for orthopedic implant application enhanced corrosion and tribocorrosion properties by nitrogen ion implantation, Appl. Surf. Sci. 347 (2015) 23–34.
[32] Q. Wang, X. Zhang, C. Huang, Y. Luo, Ion nitriding CoCrMo alloy for orthopedic applications studied by X-ray photoelectron spectroscopy analysis and tribocorrosion behavior, J. Tribol. 139 (1) (2016), 011104.
[33] G. Zhao, R.E. Aune, N. Espallargas, Tribocorrosion studies of metallic biomaterials: the effect of plasma nitriding and DLC surface modifications, J. Mech. Behav. Biomed. Mater. 63 (2016) 100–114.
[34] A.P. Ehiasarian, R. Tietema, R. Bugyi, A. Klimczak, P. Eh. Hovsepian, D. Doerwald, A Vacuum Treatment Apparatus, a Bias Power Supply and a Method of Operating a Vacuum Treatment Apparatus, Patent No ZL200780012990.9, 2011.
[35] Y.P. Purandare, G.L. Robinson, A.P. Ehiasarian, P.E. Hovsepian, Investigation of High Power Impulse Magnetron Sputtering deposited nanoscale CrN/NbN multilayer coating for tribocorrosion resistance, Wear 452–453 (2020), 203312.
[36] A. Oladokun, R.M. Hall, A. Neville, M.G. Bryant, The evolution of subsurface micro-structure and tribo-chemical processes in cocrmo-ti6al4v fretting-corrosion contacts: what lies at and below the surface? Wear 440–441 (2019), 203095.
[37] F. Liu, S. Williams, J. Fisher, Effect of microseparation on contact mechanics in metal-on-metal hip replacements-A finite element analysis, J. Biomed. Mater. Res. 103 (6) (2015) 1312–1319.
[38] F. Liu, I.J. Udofia, Z.M. Jin, F. Hirt, C. Rieker, P. Roberts, P. Grigoris, Comparison of contact mechanics between a total hip replacement and a hip resurfacing with a metal-on-metal articulation, Proc. Inst. Mech. Eng. Part C 219 (7) (2005) 727–732.
[39] W.M. Rainforth, P. Zeng, L. Ma, A.N. Valdez, T. Stewart, Dynamic surface microstructural changes during tribological contact that determine the wear behaviour of hip prostheses: metals and ceramics, Faraday Discuss 156 (0) (2012) 41–57.
[40] S. Mischler, Triboelectrochemical techniques and interpretation methods in tribocorrosion: a comparative evaluation, Tribol. Int. 41 (7) (2008) 573–583.
[41] J.R. Goldberg, J.L. Gilbert, Electrochemical response of CoCrMo to high-speed fracture of its metal oxide using an electrochemical scratch test method, J. Biomed. Mater. Res. 37 (3) (1997) 421–431.
[42] X. Luo, X. Li, Y. Sun, H. Dong, Tribocorrosion behavior of S-phase surface engineered medical grade Co–Cr alloy, Wear 302 (1) (2013) 1615–1623.
[43] T. Hanawa, S. Hiromoto, K. Asami, Characterization of the surface oxide film of a Co–Cr–Mo alloy after being located in quasi-biological environments using XPS, Appl. Surf. Sci. 183 (1) (2001) 68–75.
[44] K. Shukla, Y. Purandare, A. Sugumaran, D. Loch, A. Ehiasarian, I. Khan, P. Hovsepian, A new approach towards performing plasma nitriding of CrCoMo medical grade alloys using HIPIMS discharge, in: 64th Annual Technical Conference Proceedings, 2021.